Impact of binder concentration and pressure on performance of symmetric CNFs based supercapacitors

Article *in* Electrochimica Acta · May 2017

DOI: 10.1016/j.electacta.2017.05.186

6 authors, including:

Allan Daraghmeh
University of Barcelona
6 PUBLICATIONS **19** CITATIONS
SEE PROFILE

Shahzad Hussain
Ulster University
32 PUBLICATIONS **234** CITATIONS
SEE PROFILE

Llorenç Servera
Escola Universitària Salesiana de Sarrià
14 PUBLICATIONS **20** CITATIONS
SEE PROFILE

Elena Xuriguera
University of Barcelona
34 PUBLICATIONS **295** CITATIONS
SEE PROFILE

Electrochimica Acta 245 (2017) 531–538

Contents lists available at ScienceDirect

Electrochimica Acta

journal homepage: www.elsevier.com/locate/electacta

Impact of binder concentration and pressure on performance of symmetric CNFs based supercapacitors

Allan Daraghmeh[a,b,c,*], Shahzad Hussain[a,b], Llorenç Servera[a,d], Elena Xuriguera[a,b], Albert Cornet[a,b], Albert Cirera[a,b]

[a] MIND, Engineering Department: Electronics, Universitat de Barcelona, Martí i Franquès 1, 08028, Barcelona, Spain
[b] Institute of Nanoscience and Nanotechnology (IN2UB), Universitat de Barcelona, Joan XXIII S/N, 08028, Barcelona, Spain
[c] Department of Physics, Al-Najah National University, P.O. Box 7, West Bank, Palestine
[d] EUSS, Passeig Sant Joan Bosco,74, 08217 Barcelona Spain

ARTICLE INFO

Article history:
Received 2 March 2017
Received in revised form 26 May 2017
Accepted 28 May 2017
Available online 30 May 2017

Keywords:
Carbon nanofibers
PVDF concentration
Pressure
SEM
BET

ABSTRACT

This paper discussed in details the impact of binder polyvynilidene fluoride (PVDF) concentrations (5, 10 and 20 wt%) and pressures (~382 ~ 891 ~1783 and ~2547 MPa) for the fabrication of electrodes based on Carbon nanofibers (CNFs) for supercapcitors. The surface area, pore size distribution and morphology were characterized by Brunauer–Emmett–Teller (BET) method and SEM. The decrease in specific surface area was about 31% and pore volume 14.6% with increase in PVDF concentration from 5 to 20 wt% at ~891 MPa pressure. The assembled electrodes were tested with two electrode system in aqueous electrolyte. The specific capacitance was 80 F/g for lowest concentration of PVDF (5 wt%) and decreased about 28.3% with increase concentrations at same pressure ~891 MPa. In comparing the effect of pressure on specific capacitance, it increases about 38% for (PVDF, 10 wt%; pressure ~1783 MPa) from (PVDF, 10 wt %; pressure ~891 MPa); their corresponding power density 24502 W/kg at energy density of 6.8 Wh/Kg and 19886 W/kg at energy density energy of 3.8 Wh/kg. ESR values increase from 0.3 to 1.9 Ω with increase in PVDF concentration and decrease again to 0.5 Ω with increase in pressure. The results show optimal conditions are 10 wt% of PVDF and higher pressure of ~891 MPa.

1. Introduction

The current research and development efforts on electrochemical power sources are mainly focused on fuel cell, electrochemical capacitors and are directed towards achievement of high specific energy, high specific power, long cycle life, at relative low cost [1–3]. Most of supercapacitor electrodes include carbon material like activated Carbon (AC), Carbon nanofibers (CNFs), Carbon nanotubes (CNTs) or Graphene because of good electric conductivity, high surface area and large specific capacitance [4–10]. The charge stored for carbon material at electrode/electrolyte interface produce high capacitance because of high surface area [10,11].

CNFs have been receiving higher attention for use it as electrodes in supercapacitors because of their high length to diameter ratio, high surface area and excellent electric conductivity. CNFs could be defined as sp^2-based linear filaments with diameter of ~100 nm that are characterized by flexibility and their aspect ratio (above 100) [12,13]. Since CNFs could be considered as the 1-D form of carbon, their structure and properties are closely related to those of other forms of carbon, especially to crystalline three-dimensional graphite, turbostratic carbons, and to their constituent 2-D layers [3,14]. The fabrication of CNFs based electrodes for supercapacitors requires a binder to join them together forming a compact layer and adhere homogeneously onto the current collector [15]. Various types of polymers such as polyvynilidene fluoride (PVDF), polyvynilidene chloride (PVDC) and Teflon [10], are commonly used in proportions that usually vary from 5 to 10 wt. % [16–18]. The main role of binder is to provide enough strength during the electrode formation and appropriate pore sizes. The amount of binder therefore should be kept as low as possible, in order not to reduce surface area or conductivity in the electrode. At the same time, enough polymer should be added to ensure that CNFs are compact and so that the electrode is manageable [19]. The porous carbon material having dominant pores in the range 0.7–1 nm size exhibits excellent performance of forming double layer in aqueous electrolyte [16,17]. However, binders inevitably cover some surface areas or pores of active materials, which block the paths for ions to move

* Corresponding author.
E-mail address: allan.daraghmeh@ub.edu (A. Daraghmeh).

http://dx.doi.org/10.1016/j.electacta.2017.05.186
0013-4686/

inside the pores. It is important to find a relationship between the amounts of binder usage for the preparation and pore size distribution as well as its impact on the electrochemical properties of electrode. PVDF is a semi-crystalline fluoropolymer that presents high mechanical stability, proper swelling properties and extraordinary performance due to high integration within electrodes. PVDF combines the active materials to each other to form the electrode material [20]. The PVDF polymer has a typical stability of fluoropolymers but interactive groups will produce a unique polarity, thus results in its good chemical and oxidative resistances, poor hydrophilicity and significant swelling property in the electrolyte. Compared to other fluoropolymers, like polytetrafluoroethylene (Teflon), PVDF has a low density (1.78 g/cm^3). Besides PVDF does not dissolve in the aqueous electrolyte like PVA [21]. For all these reasons PVDF could be a suitable polymer for carbonaceous electrodes in supercapacitors.

Recently the optimal content of PVDF for the preparation of AC electrodes was found 5 wt% [21]. In fact, Zhu and coworkers found the highest capacitance in AC electrodes blended with PVDF at 5% among different concentrations of PTFE and Nafion [21]. Generally, supercapacitor electrodes are manufactured by printing/brushing slurry on a substrate or using pressure force. Li-Feng Chen et al. manufactured CNFs based electrodes by using 10 MPa pressure [22]. V. Barranco at al. prepared CNFs electrode by using force of 2 ton/cm^2 for 2 min [23]. C Xu et al. fabricated AC electrodes at 80 °C under 100 MPa on a titanium plate [24]. Q Abbas et al. pressed AC power by 5 ton/cm^2 force to make pellets [20]. As far as we know there is no systematic study concerning the testing of various PVDF % weight and hydro pressure force to fabricate electrodes based on CNFs.

In our work the two objectives were chosen to study the electrochemical properties of CNFs, first the effect polymer concentration with 5, 10 and 20 wt% PVDF, and second the influence of various pressures to manufacture the pellets (∼382 ∼ 891, ∼1783 and ∼2547 MPa).

2. Experimental procedure

2.1. Electrode Preparation

Symmetric supercapacitor based CNFs were fabricated with different concentration of PVDF for comparison. CNFs were provided by Grupo Antolin (GANF). It has a helicoidally graphitic stacked cup structure, there is a presence of Ni (6%), diameter is 20–80 nm, length >30um, electric resistivity $10^{-2}\,\Omega$cm. The electrode preparation for supercapacitor was achieved by milling of CNFs in a zirconia ball mill employing a frequency 500 rpm for 30 minutes in a Fritch Pulverisette 7 planetary milling. PVDF was used as a binder. Mixed CNFs were joint together using different concentration of PVDF in solution of 15 ml of acetone in agate mortar. The slurry was then mixed using a mechanical stirrer for 1 hour, and this was followed by an ultrasonic for 30 minutes. The slurry was dried in vacuum oven at 70 °C for 1 h. The dried sample was then used to assemble the supercapacitores electrode. The samples of CNFs/PVDF were pressed using hydraulic press at different pressures (∼382, ∼891, ∼1783 and ∼2547 MPa).

The prepared samples with PVDF concentration of (5, 10 and 20 wt%) with pressure ∼891 MPa are designated as wt-5, wt-10 and wt-20 and alone CNFs without PVDF are named as wt-0. The influence of pressure to prepare the electrode disc was investigated in the range (∼382 to ∼2547) MPa. At lower pressure (∼382 MPa) it was difficult to fabricate the disc due to lack of powder adhesion and at higher pressure (∼2547 MPa) the electrode disc was broken. We were able to prepare the electrode discs at ∼891 and ∼1782 MPa. These samples were prepared using concentrations 10 wt% of PVDF. The sample manufactured with ∼891 MPa pressure designated as wt-10 and with ∼1783 MPa pressure, as wt-10-1. It was noticed that thickness of discs decreases from 0.55 mm to 0.33 mm for ∼891 MPa to ∼1783 MPa. The mass of all the prepared electrode discs was ∼20 mg. Fig. 1 (a) shows a prepared disc of CNFs electrode.

2.2. Characterization

The samples were examined by scanning electron microscopy (SEM) (Jeol J-7100). The porous texture, specific surface area and pore size distribution (BET) of CNFs with different concentration of binder PVDF were obtained by physical adsorption of N_2 at 77 K using an automated gas adsorption analyzer (Micromeritics TriStar 3000 V6.04 A). All samples were outgassed at 100 °C for 4 h prior to the adsorption measurements.

The electrochemical performance CNFs symmetric supercapacitors were studied in two electrode Swagelok cell and using a Gamry 600 potentiostat in a 6 M KOH solution as an electrolyte. The specific capacitance of electrode materials was investigated by: cyclic voltammetry (CV), galvanostatic charging/discharging (GCD) and electrochemical impedance spectroscopy (EIS).

3. Results and discussion

3.1. Morphological characterization

The surface morphology of prepared electrodes was examined by SEM, see Fig. 1. It can be seen that PVDF binder effectively bonds the CNFs Fig. 1(b, c). The different structures for the electrodes of CNFs with and without PVDF are visible. It was also observed that increasing pressure from ∼891 MPa to ∼1782 MPa, the CNFs become more compact.

3.2. Surface area and Pore texture of CNFs

The specific surface area and pore size distribution of CNFs electrodes prepared with different concentration of polymer PVDF were obtained from the N_2 adsorption/desorption. The N_2 adsorption/desorption isotherm of CNFs without PVDF (wt-0) and with different concentration of PVDF are shown in Fig. 2(a). The isotherm of wt-0 shows the adsorbed volume is higher than others. The isotherms of CNFs for all samples present a small hysteresis loop in middle pressure range from 0 to 0.45, which

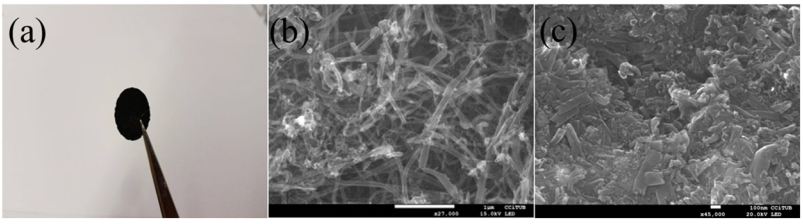

Fig. 1. Photograph of prepared electrode disc (a), SEM images of CNFs, (b) without PVDF (wt-0), (c) with PVDF (wt-20).

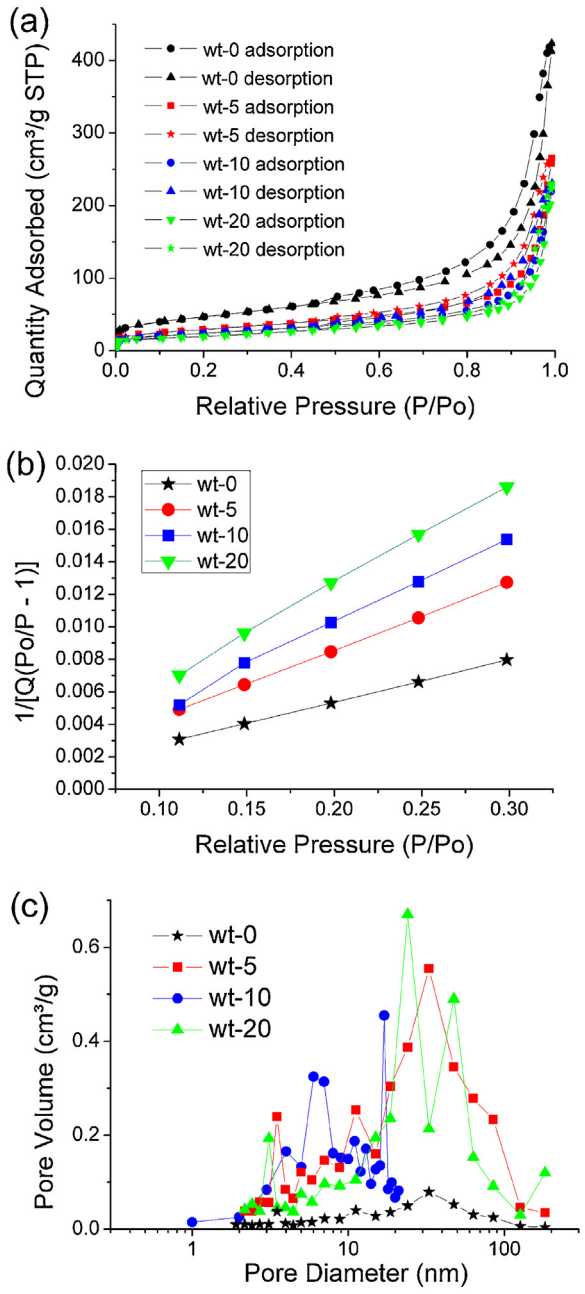

Fig. 2. (a) Nitrogen adsorption/desorption isotherms, (b) BET surface area, (c) Pore size distribution calculated by BJH Desorption dV/dlog(D) Pore Volume.

indicates CNFs contain mesoporous and macro pores structure. According to IUPAC classification the isotherm of all samples can be classified as type II isotherm [25]. The pore distribution of CNFs for all sample are listed in Table 1.

The BET specific surface area is extracted from the linear region of $1/[Q_m(p_0/p-1)]$ versus p/p_0 in the classical BET range of 0.1–0.3 Fig. 2(b). CNF without PVDF (wt-0) hold surface area 165 m^2/g. The sample wt-5 contains surface area of 103 m^2/g while wt-10 and wt-20 have surface areas of 86 m^2/g and 71 m^2/g respectively. The decrease in specific surface area is (37.57 to 57%) when CNFs mixed with PVDF (5 to 20 wt%). The total volume of pores (V_t, cm^3/g) was calculated by the number of adsorbed nitrogen at $P/P_0 \approx 0.9932$. The volume of micropores and the values of surface areas of micro (S_{micro}, m^2/g) were investigated by the use of t-Plot Harkins and Jura method. The pore size distribution of CNFs without and with different concentration of PVDF sample calculated from adsorption isotherms by the Barrett–Joyner–Halenda (BJH) method. The total pore volumes are 0.654, 0.41, 0.356 and 0.35 cm^3/g for wt-0, wt-5, wt-10 and wt-20 respectively at relative pressure ($P/P_0 = 0.9932$). These results indicate that with increase in PVDF concentration most of the pores get blocked which do not contribute during the measurements of surface area.

The pore size distribution of the materials is classified into three groups: micro pores (<2 nm), meso pores (2–50 nm) and macro pores (>50 nm) [26]. Fig. 2(c) exhibits pore size distribution of CNFs mixtures. CNFs without PVDF (wt-0) contain 9.2% (micropores), 44.6% (mesopores) and 46.2% (macropores). CNFs electrode manufactured with 5 wt% (wt-5) contains 0.72% (micropores), 72% (mesopores) and 27.3% (macropores). It was observed with increase in PVDF concentrations for samples wt-10 and wt-20, micro and mesopores contribution decreases and the external surface area increases, as shown Table 1. These finding tells that higher PVDF concentration blocks small sizes of pores which are also the result of decrease in surface area. It was observed that there was no difference in the surface area or pore size distribution for wt-10 and wt-10-1 even when the electrodes were prepared with different pressures. This is because for BET analysis it was needed to break the electrode to make in powder form.

3.3. Electrochemical measurement

The electrochemical properties of supercapacitor were tested based on two electrode cell systems, which can measure their performance more accurately [27]. The cyclic voltammetry analysis of supercapacitor is a basic technique to understand the electrochemical performance of the electrode material. The specific capacitance per unit mass for one electrode was calculated using Eq. (1).

$$C_s = 4 * C/m \tag{1}$$

$$C = \frac{q_a + |q_c|}{2\Delta V} \tag{2}$$

Where C_s is the specific capacitance in F/g, q_a and q_c are the anodic and cathodic charges, C is the measured capacitance for the two-electrode cell by equation 2 and m is the total mass of the active material in both electrodes [28].

Fig. 3(a) presents the comparison of cyclic voltammograms (CVs) for the samples at a scan rate 5 mV/s. The CVs display rectangular shape without any redox active peaks which is a signature of excellent double layer behavior. Fig. 3(b) shows the specific capacitance comparison for different scan rates. It can be seen that sample wt-10-1 gives higher specific capacitance 96 F/g at scan rate 5 mV/s. It was found 64% specific capacitance retention at high scan rate (500 mV/s). For the sample wt-5 the specific capacitance decreases from 80 to 50 F/g for scan rate 5 to 500 mV/s respectively. The other two samples wt-10 and wt-20 delivers the specific capacitance of 59 and 57 F/g respectively at scan rate 5 mV/s, which are much lower than others. Comparing only PVDF concentration, the sample prepared with lowest concentration (5 wt%) shows higher capacitance over the others at all scan rate, but it was observed that pressure also make a significant effect on the properties of supercapacitor. The sample wt-10-1 prepared with 10 wt% and 1783 MPa pressure shows highest specific capacitance and retention at all scan rate. This could mean that even at higher scan rate the interior micropores are accessible to the ions. The electrochemical analysis correlation with surface texture, pore size distribution and thickness of electrode evaluate the performance of supercapacitor. The BET specific surface area drops down about 31% with increase in PVDF binder concentration. PVDF is a hydrophobic agent, this nature of binder makes the

Table 1
Physicochemical parameters of CNFs electrode prepared with different concentration of PVDF at constant pressure ~891 MPa.

Sample	SSA[a] (m^2/g)	V_t[b] (cm^3/g)	V_{Micro}[c] (cm^3/g)	V_{Meso}[d] (cm^3/g)	V_{Macro}[e] (cm^3/g)	P_{Micro}[f] (%)	P_{Meso}[g] (%)	P_{Macro}[h] (%)	Ext_{area}[i] (m^2g)	C_{sp} (F/g)
Wt-0	165	0.654	0.06	0.29	0.3	9.2	44.6	42.2	155	–
wt-5	103	0.4	0.00288	0.285	0.109	0.72	72	27.3	97	80
wt-10	86	0.356	0.00233	0.244	0.11	0.65	68.4	30.8	80	59
wt-20	71	0.35	0.00042	0.184	0.166	0.12	52.4	47.4	68	57.3

[a] specific surface area.
[b] Single point volume adsorption total volume of pores at p/p0=0.9932.
[c] micro volume from t-plot (y-intercept).
[d] Meso volume from BJH method.
[e] Macro Volume by BJH method.
[f] The micro, meso and macro percentage calculated by V_{MICR}/V_{TOTAL}*100%, V_{MESO}/V_{TOTAL}*100%.
[g] The micro, meso and macro percentage calculated by V_{MICR}/V_{TOTAL}*100%, V_{MESO}/V_{TOTAL}*100%.
[h] The micro, meso and macro percentage calculated by V_{MICR}/V_{TOTAL}*100%, V_{MESO}/V_{TOTAL}*100%.
[i] EXT (External area) area from the slope of t −plot. Csp (Specific capacitance at scan rate 5 mV/s).

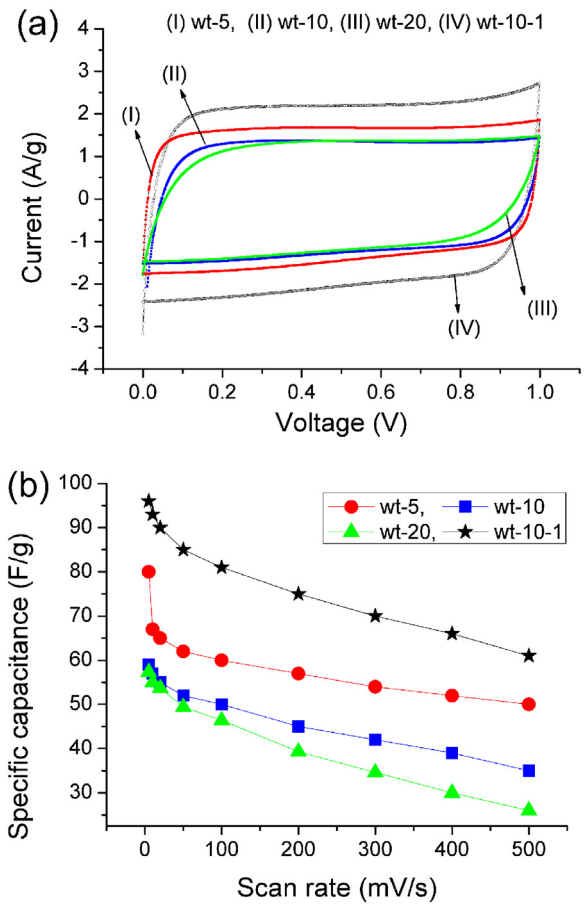

Fig. 3. (a) CV comparison at scan rate 5 mV/s, (b) Evolution of the specific capacitance at different scan rates.

carbon electrode more hydrophobic which makes it difficult for ions to penetrated deep inside the pores of electrode when using aqueous electrolyte. As a result decrease in the ion mobility, the electrode performance will be reduced. In addition from BET results it was found with increase in PVDF concentration the (micro, mesopore %) volume and surface area decreases. The increase in the pressure from ~891 MPa to ~ 1783 MPa decreases the thickness of electrode from 0.55 mm to 0.33 mm. It is known that relationship between density and volume is inversely proportional at constant mass. As the thickness (volume) decreases the density of the CNFs is increased. This lessening of thickness diminishes the space between the pores and outer area which can make significant impact in increase specific capacitance. All of above mentioned properties make a significant influence on the specific capacitance of electrode according to the equation.

$C = \in A/d$. Where A is the specific surface area of the electrode accessible to the electrolyte ions, and d is the effective thickness of the EDL (the Debye length) [29].

Once studied the Faradic behavior of the supercapacitors we wonder about the stability. Figure supplementary information SI (a) shows cyclic voltammograms of the sample wt-5 measured at different scan rates from 5 mV/s to 500 mV/s. The rectangular shapes of CV curves at all scan rates tell about the excellent conductivity and low mass transport resistance [30]. The cycling stability test for up to 100 cycles at a high scan rate 200 mV/s is presented in figure SI (b). The 100 CVs are overlapping each other, which mean stable capacitance behavior.

The dynamics of the charge and discharge where investigated through galvanostatic charge discharge (GCD). Fig. 4(a) shows a comparison of the GCD curves at a constant current density of 0.45 A/g in the potential range of 0–1 V. As can be seen all samples show a similar symmetrical triangular curve with a nearly linear variation of voltage as a function of time during charge and discharge but different IR drop values. This type of curve is typical for CNFs based supercapacitors [5]. The data shows that all three concentrations of PVDF and different pressures based supercapacitors present good performance. However, despite having similar shape the curve for the sample wt-10-1 took significantly longer charge and discharge times, which indicates that higher number of electrons and electrolytes ions are participating in charge and discharge process.

Fig. 4(b) shows GCD curves recorded at different current densities for sample wt-5. The nearly symmetric rectangular shapes of charge/discharge curves indicate the high and reversible charge storage capacity of CNFs. It has been reported that appearance of the IR drop is the consequence of combined resistance of solution, electrode and ion migration in the electrode [31,32]. IR drop was enhanced with increase in the current density. Fig. 4(c) shows the plotted graph between discharge currents and IR drops. The slope of the diagram could be used to estimate the overall resistance of the capacitor: the higher the slope, the greater the overall resistance of the capacitor [28]. The slopes have a trend like wt-10–1 < wt–5 < wt–10 < wt-20. It can be suggested that higher pressure can significantly reduce the resistance of the capacitor, which is a worth to increase supercapacitor performances.

The discharge capacitance (C) is estimated from the slope (dV/dt) of the linear portion of the discharge curve using equation 3.

$$C_s = \left(\frac{2I}{(dV/dt).m}\right) \quad (3)$$

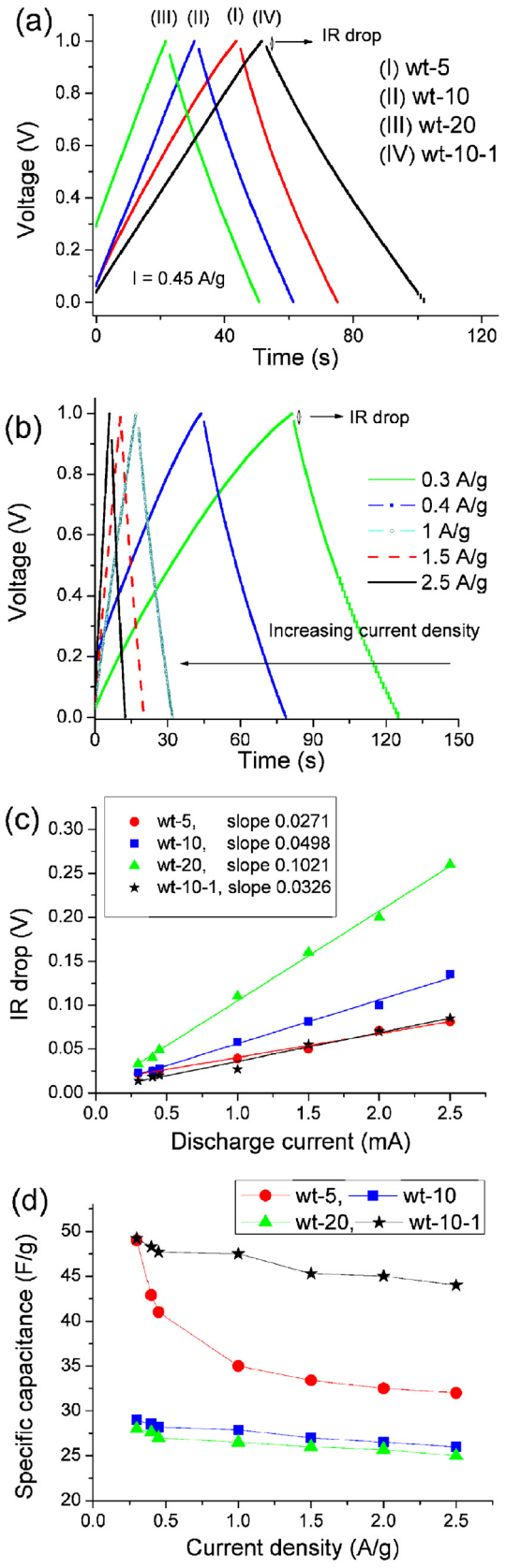

Fig. 4. (a) Charge/discharge comparison at a constant current density of 0.45 A/g, (b) charge/discharge curves for wt-5 at different current densities, (c) Variation of IR drop with discharge currents, (d) specific capacitance comparison at different current densities.

Where C_s is the specific capacitance in F/g, ΔV is the voltage difference during the discharge curve in V, I is the current in A and Δt the discharge time in s, m is the mass of both electrodes.

Fig. 4(d) shows the variation of the specific capacitance with current density. The specific capacitance of wt-10-1 decrease from 49.2 to 44 F/g for current densities 0.3 to 2.5 A/g respectively, indicates small decrease in capacitance even at higher current densities. Whereas a big drop in specific capacitance was observed for wt-5 from 49 to 32 F/g with increase in current density. The other two samples also present decrease in specific capacitance with increase in current density.

The charge discharge cycling stability up to 2000 cycles was tested at affixed current density 1.5 A/g Fig. 5(a). The capacitance was calculated by using equation 3. All samples show almost constant capacitance from the first to the last cycle. The specific capacitance follow the trend like wt-10–1 < wt–5 < wt–10 < wt-20. The specific energy density is defined as the amount of energy stored per unit weight in a particular device, while specific power density is directly related to the rate at which energy can be transferred from the device [33].

The maximum power density (P) and energy density (E) delivered upon discharge were estimated by Eqs. (4) and (5).

$$P = \frac{V^2}{(4.ESR.m)} \tag{4}$$

$$E = \frac{1}{2}CV^2 \tag{5}$$

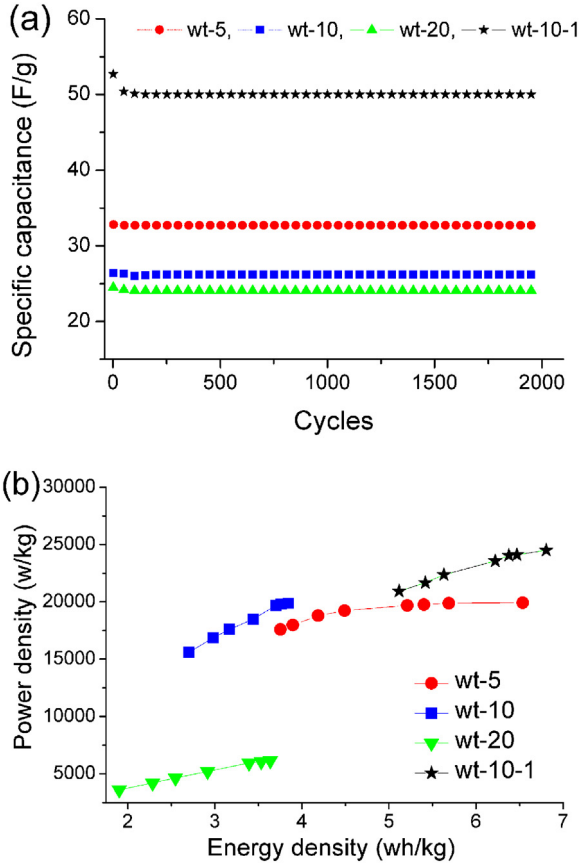

Fig. 5. (a) Charge/discharge cycling stability at constant current density 1.5 A/g, (b) Ragone plot of power density against energy density.

Where V is the voltage excluding IR drop, ESR obtained by EIS analysis, m mass of active material, C is capacitance calculated by GCD.

Fig. 5(b) shows the samples comparison with respect to power density and energy density. The sample wt-5 delivers energy density of 6.53 Wh/kg and power density of 19927 W/kg at current density of 1 A/g. The sample wt-10 presents energy density and power density (3.8 Wh/kg, 19886 W/Kg) at current density of 1 A/g and (2.7 Wh/kg, 15886 W/kg) at 4.5 A/g. The sample wt-10-1 prepared with higher pressure force delivers significantly higher energy density and power density (6.8 Wh/kg, 24502 W/kg) at current density of 1 A/g and (5.1 Wh/kg, 20930 W/kg) at 4.5 A/g. These results show, with increase energy density, the power density is almost constant or decreases a little bit, which are a signature of excellent electrochemical properties of high energy density and power output, therefore very promising for application in the scenarios where high power output as well as high energy capacity is required [34]. The other samples present smaller power and energy then the wt-10-1.

AC impedance spectroscopic measurements were performed to investigate the electrochemical characteristics of the symmetric supercapacitors. Fig. 6(a) shows the Nyquist plot for all the samples. The impedance measurements were carried out at AC with 10 mV amplitude over a frequency range between 100 kHz to 0.1 Hz. Generally the complex plane of impedance (Nyquist) plot of porous electrode consists on a high frequency semicircle, a 45° region (Warburg region) of transition between high and low frequencies, and almost a vertical line at low frequencies [3]. The equivalent series resistance (ESR) comprises on contact resistance, solution resistance, and charge transfer resistance of the electrode material. The appearance of Warburg region is the consequence of the combination of resistive and capacitive behaviors of the ions penetrating into the electrode pores [35]. It can be seen from Fig. 6(a) that all the samples show a semicircle in the high frequency region and a straight line in the lower frequency region. This indicates that the supercapacitors have a blocking behavior at high frequencies and a capacitive behavior at low frequencies. A very big semicircle from high to mid frequency is observed for the sample wt-20, which indicates high intrinsic resistance (charge transfer resistance) of porous structure [36]. It can be seen that for the four samples intrinsic resistance of electrodes are in the order of wt% that is wt–5 < wt-10–1 < wt–10 < wt-20. The reason might be that higher polymer concentration would block the conductive paths of the pores. However, with higher pressure ~1783 MPa intrinsic resistance values decreases. The possible reason behind this could be a decrease in the thickness of electrode means reduce in the space between the pores which effectively reduced the intrinsic resistance. The equivalent series resistance (ESR) values of the electrode material are (0.3, 0.6, 1.9 and 0.5 (Ω)) for wt-5, wt-10, wt-20 and wt-10-1 respectively. These results tell that electrical conductivity decrease with increase in the PVDF concentration, whereas pressure reduces it.

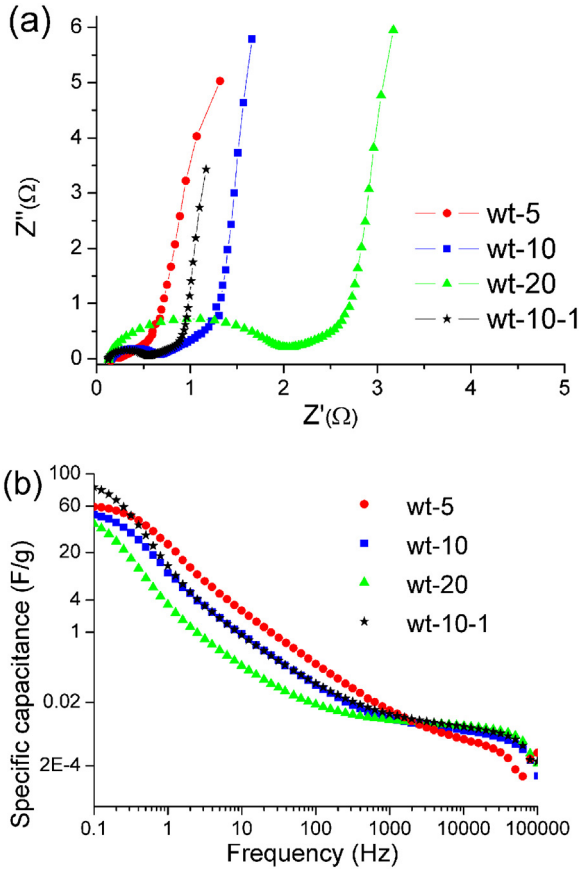

Fig. 6. (a) Nyquist plot for all samples, (b) Specific capacitance comparison calculated from EIS.

The specific capacitance of the samples were calculated from the impedance analysis employing the imaginary component of impedance by following Eq. (6) [37].

$$C_s = 4(-(1/2\pi f z'' m)) \quad (6)$$

where f is frequency in Hz. z'' is the imaginary component of impedance and m, the mass of CNFs or AC calculated for one electrode. Fig. 6(b) shows that the change in the specific capacitance of electrodes mainly below the frequency of 1500 Hz. The obtained specific capacitances at low frequency 0.1 Hz for wt-5, wt-10, wt-20 and wt-10-1 are 59.2, 50.8, 41.6, 83 F/g respectively.

Fig. 7 (a) was used to evaluate the relaxation time constant. The relaxation time constant represents the transition of electrochemical capacitor from purely resistive to purely capacitive and can be calculated by using $\tau_0 = {}^{1}/_{f_k}$, where f_k is the knee frequency at phase shift 45° [38]. The relaxation time constant were 1, 2, 5 and 2.5 s for wt-5, wt-10, wt-20 and wt-10-1 respectively. It shows that relaxation time constant increased with increase in PVDF concentration but decreased again with increase in pressure.

Our results show much lower values of time constant in comparing other reports [35,39]. R Farma et al. obtained τ_0 values 25.12 and 50.13 s for carbon electrode based on carbon nanotubes and biomass carbon [35]. T Thomberg et al. results show the τ_0 values in the range of 3 to 68 s for carbon electrodes manufactured from micro/mesoporous carbon [39]. Fig. 7(b) represents the variation of phase angle as a function of frequency, which is known as Bode plot. The phase angles at low frequency 0.1 Hz are found −75°, −74°, −60° and 75.3 for wt10-1 respectively. These values are close to −90° which means better capacitive performance and rapid charge discharge process.

4. Conclusions

CNFs based symmetric supercapacitors have been prepared and test with different concentration of PVDF and pressure forces. The highest surface area decreases about 31% and percentage of (micro, meso) volume decreases with increase in concentration of PVDF (5 to 20 wt%). Cyclic voltammetry, constant current charge/discharge and electrochemical impedance spectroscopy methods have been used to evaluate the electrochemical characteristics. Highest specific capacitance (96 F/g) was achieved with 10 wt% of PVDF, and a pressure of ~1783 MPa. The comparison between lower to higher pressures indicate higher pressure decrease the thickness of

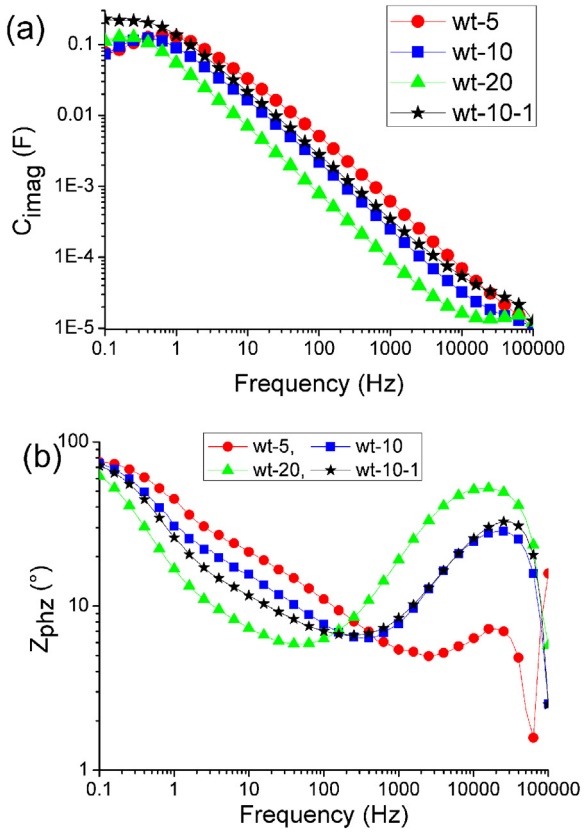

Fig. 7. (a) Imaginary capacitance as function of frequency, (b) the relation of phz angle vs frequency.

electrode and this play important role in increasing the capacitance. The power density and energy density was higher with lower concentration of PVDF as well as when higher pressure was used. Impedance spectroscopy results reveal the ESR values increase from 0.3 to 1.9 Ω with increase in PVDF and decrease again to 0.5 Ω with increase in pressure. Our results show best parameters are 10 wt% of PVDF and higher pressure of ~1783 MPa.

Acknowledgements

A. Daraghmeh acknowledges the European Union grant for PhD grant in Erasmus Mundus AVEMPACE III program. A. Cirera acknowledges 2015 edition of BBVA Foundation Grants for Researchers and Cultural Creators. Grupo Antolín Ingeniería, S.A. is acknowledged for supplying CNF, GO and rGO samples. Authors thank MINECO for grant MAT2015-66443-C2-2-R.

Appendix A. Supplementary data

Supplementary data associated with this article can be found, in the online version, at http://dx.doi.org/10.1016/j.electacta.2017.05.186.

References

[1] B.E. Conway, V. Birss, J. Wojtowicz, The role and utilization of pseudocapacitance for energy storage by supercapacitors, Journal of Power Sources 66 (1997) 1.
[2] J.P. Zheng, T.R. Jow, A New Charge Storage Mechanism for Electrochemical Capacitors, J. Electrochem. Soc. 142 (1995) L6–L8.
[3] R. Kotz, M. Carlen, Principles and applications of electrochemical capacitors, Electrochimica Acta 45 (2000) 2483–2498.
[4] H. Shen, E. Liu, X. Xiang, Z. Huang, Y. Tian, Y. Wu, Z. Wu, H. Xie, A novel activated carbon for supercapacitors, Materials Research Bulletin 47 (2012) 662–666.
[5] A. Daraghmeh, S. Hussain, L. Servera, E. Xuriguera, M. Blanes, F. Ramos, A. Cornet, A. Cirera, Flexible supercapacitors based on low-cost tape casting of high dense carbon nanofibers, Mater. Res. Express 4 (2017) 025007.
[6] S. Hussain, R. Amade, E. Jover, E. Bertran, Nitrogen plasma functionalization of carbon nanotubes for supercapacitor applications, J. Mater. Sci. 18 (2013) 7620–7628.
[7] C.M. Ghimbeu, E. Raymundo-Piñero, P. Fioux, F. Béguin, C. Vix-Guterl, Vanadium nitride/carbon nanotube nanocomposites as electrodes for supercapacitors, J. Mater. Chem. 21 (2011) 13268–13275.
[8] C. Zhu, T. Liu, F. Qian, T. Yong-Jin Han, E.B. Duoss, J.D. Kuntz, C.M. Spadaccini, M. A. Worsley, Y. Li, Supercapacitors Based on Three-Dimensional Hierarchical Graphene Aerogels with Periodic Macropores, Nano Lett. 16 (2016) 3448–3456.
[9] Zhong-Shuai Wu, K. Parvez, X. Feng, K. Mullen, Graphene-based in-plane micro-supercapacitors with high power and energy densities, Nature Communications 4 (2013), doi:http://dx.doi.org/10.1038/ncomms3487 Article number: 2487.
[10] Q.Y. Li, Z.S. Li, L. Lin, X.Y. Wang, Y.F. Wang, C.H. Zhang, H.Q. Wang, Facile synthesis of activated carbon/carbon nanotubes compound for supercapacitor application, Chem. Eng. J. 156 (2010) 500–504.
[11] J.M. Ko, K.M. Kim, Electrochemical properties of MnO_2/activated carbon nanotube composite as an electrode material for supercapacitor, Mater. Chem. Phys. 114 (2009) 837–841.
[12] O. Monereo, S. Illera, A. Varea, M. Schimidt, T. Sauerwald, A. Schütze, A. Cirera, J.D. Prades, Localized self-heating in large arrays of 1D nanostructures, Nanoscale 8 (2016) 5082–5088.
[13] S. Claramunt, O. Monereo, M. Boix, R. Leghrib, J.D. Prades, A. Cornet, P. Merino, C. Merino, A. Cirera, Flexible gas sensor array with an embedded heater based on metal decorated carbon nanofibres, Sens. Actuator B 187 (2013) 401–406.
[14] J.B. Donnet, R.C. Bansal, Carbon Fibers, MarcelDekker, New York, 1984.
[15] Keh-Chyun Tsay, L. Zhang, J. Zhang, Effects of electrode layer composition/thickness and electrolyte concentration on both specific capacitance and energy density of supercapacitor, Electrochimica Acta 60 (2012) 428–436.
[16] E. Frackowiak, F. Béguin, Carbon materials for the electrochemical storage of energy in capacitors, Carbon 39 (2001) 937–950.
[17] K.H. An, W.S. Kim, Y.S. Park, Y.C. Choi, S.M. Lee, D.C. Chung, D.J. Bae, S.C. Lim, Y. H. Lee, Supercapacitors Using Single-Walled Carbon Nanotube Electrodes, Advanced Materials 13 (2001) 497–500.
[18] S. Shiraishi, H. Kuriharea, A. Oya, Preparation and Electric Double Layer Capacitance of Mesoporous Carbon, Carbon Sicence 1 (2001) 133–137.
[19] V. Ruiz, C. Blanco, M. Granda, R. Menéndez, R. Santamaría, Influence of electrode preparation on the electrochemical behaviour of carbon-based supercapacitors, Appl Electrochem 37 (2007) 717–721.
[20] Q. Abbas, D. Pajak, E. Frąckowiak, F. Béguin, Effect of binder on the performance of carbon/carbon symmetric capacitors in salt aqueous electrolyte, Electrochimica Acta 140 (2014) 132–138.
[21] Z. Zhu, S. Tang, J. Yuan, X. Qin, Y. Deng, R. Qu, G M Haarberg Effects of Various Binders on Supercapacitor Performances, Int. J. Electrochem. Sci. 11 (2016) 8270–8279.
[22] Li-Feng Chen, Xu-Dong Zhang, Hai-Wei Liang, Mingguang Kong, Qing-Fang Guan, Ping Chen, Zhen-Yu Wu, Shu-Hong Yu, Synthesis of Nitrogen-Doped Porous Carbon Nanofibers as an Efficient Electrode Material for Supercapacitors, ACS Nano 8 (2012) 7092–7102.
[23] V. Barranco, M.A. Lillo-Rodenas, A. Linares-Solano, A. Oya, F. Pico, J. Ibanez, F. Agullo-Rueda, J.M. Amarilla, J.M. Rojo, Amorphous Carbon Nanofibers and Their Activated Carbon Nanofibers as Supercapacitor Electrodes, J. Phys. Chem. C 114 (2010) 10302–10307.
[24] C. Xu, H. Du, B. Li, F. Kang, Y. Zeng, Asymmetric Activated Carbon-Manganese Dioxide Capacitors in Mild Aqueous Electrolytes Containing Alkaline-Earth Cations, Journal of The Electrochemical Society 156 (6) (2009) A435–A441.
[25] S.J. Gregg, K.S.W. Sing, Adsorption, Surface Area and Porosity, 2nd ed., Academic Press, New York, 1982 pp 4, 287.
[26] J. Huang, B.G. Sumpter, V. Meunier, A Universal Model for Nanoporous Carbon Supercapacitors Applicable to Diverse Pore Regimes, Chemistry 14 (2008) 6614–6626.
[27] Qiong Wu, Yuxi Xu, Zhiyi Yao, Anran Liu, Gaoquan Shi, Supercapacitors Based on Flexible Graphene/Polyaniline Nanofiber Composite Films, ACS Nano 4 (2010) 1963–1970.
[28] M.D. Stoller, R.S. Ruoff, Best practice methods for determining an electrode material's performance for ultracapacitors, Energy Environ. Sci. 3 (2010) 1294–1301.
[29] Li Li Zhang, X.S. Zhao, Carbon-based materials as supercapacitor electrodes, Chem. Soc. Rev. 38 (2009) 2520–2531.
[30] Y. Liu, J. Zhou, L. Chen, P. Zhang, W. Fu, H. Zhao, Y. Ma, X. Pan, Z. Zhang, W. Han, E. Xie, Highly Flexible Freestanding Porous Carbon Nanofibers for Electrodes Materials of High-Performance All-Carbon Supercapacitors, ACS Appl. Mater. Interfaces 7 (2015) 23515–23520.
[31] M. Endo, T. Maeda, T. Takeda, Y.J. Kim, K. Koshiba, H. Hara, M.S. Dresselhaus, J. Electrochem. Soc. 148 (2001) 910.
[32] Q. Guo, X. Zhou, X. Li, S. Chen, A. Seema, A. Greiner, H. Hou, Supercapacitors based on hybrid carbon nanofibers containing multiwalled carbon nanotubes, J. Mater. Chem. 19 (2009) 2810–2816.
[33] W.K. Chee, H.N. Lim, I. Harrison, K.F. Chong, Z. Zainal, C.H. Ng, N.M. Huang, Performance of Flexible and Binderless Polypyrrole/Graphene Oxide Zinc Oxide Supercapacitor Electrode in a Symmetrical Two-Electrode Configuration, Electrochimica Acta 157 (2015) 88–94.

[34] W. Xing, S.Z. Qiao, R.G. Ding, F. Li, G.Q. Lu, Z.F. Yan, H.M. Cheng, Superior electric double layer capacitors using ordered mesoporous carbons, Carbon 44 (2006) 216–224.
[35] R. Farma, M. Deraman, Awitdrus, I.A. Talib, R. Omar, J.G. Manjunatha, M.M. Ishak, N.H. Basri, B.N.M. Dolah, Physical and Electrochemical Properties of Supercapacitor Electrodes Derived from Carbon Nanotube and Biomass Carbon, Int. J. Electrochem. Sci. 8 (2013) 257–273.
[36] L. Li, E. Liu, H. Shen, Y. Yang, Z. Huang, X. Xiang, Y. Tian, Charge storage performance of doped carbons prepare from polyaniline for supercapacitors, J Solid State Electrochem. 15 (2011) 175–182.
[37] E.G. Calvo, F. Lufrano, P. Staiti, A. Brigandì, A. Arenillas, J.A. Menéndez, Optimizing the electrochemical performance of aqueous symmetric supercapacitors based on an activated carbon xerogel, Journal of Power Sources 241 (2013) 776–782.
[38] V. Ganesh, S. Pitchumanib, V. Lakshminarayanan, New symmetric and asymmetric supercapacitors based on high surface area porous nickel and activated carbon, Journal of Power Sources 158 (2006) 1523–1532.
[39] T. Thomberg, A. Jänes, E. Lust, Energy and power performance of electrochemical double-layer capacitors based on molybdenum carbide derived carbon, Electrochimica Acta 55 (2010) 3138–3143.